J|A|C|S
ARTICLES

Published on Web 12/22/2008

Tuning the Electronic and Molecular Structures of Catalytic Active Sites with Titania Nanoligands

Elizabeth I. Ross-Medgaarden,[†] Israel E. Wachs,[*,†] William V. Knowles,[‡]
Andrew Burrows,[§] Christopher J. Kiely,[§] and Michael S. Wong[‡,‖]

Operando Molecular Spectroscopy and Catalysis Laboratory, Department of Chemical Engineering, Lehigh University, Bethlehem, Pennsylvania 18015, Department of Chemical and Bimolecular Engineering, Rice University, Houston, Texas 77005, Departments of Materials Science and Engineering, Lehigh University, Bethlehem, Pennsylvania 18015, and Department of Chemistry, Rice University, Houston, Texas 77005

Received December 28, 2007; E-mail: iew0@lehigh.edu

Abstract: A series of supported 1−60% TiO_2/SiO_2 catalysts were synthesized and subsequently used to anchor surface VO_x redox and surface WO_x acid sites. The supported TiO_x, VO_x, and WO_x phases were physically characterized with TEM, in situ Raman and UV−vis spectroscopy, and chemically probed with in situ CH_3OH-IR, CH_3OH-TPSR and steady-state CH_3OH dehydration. The CH_3OH chemical probe studies revealed that the surface VO_x sites are redox in nature and the surface WO_x sites contain acidic character. The specific catalytic activity of surface redox (VO_4) and acidic (WO_5) sites coordinated to the titania nanoligands are extremely sensitive to the degree of electron delocalization of the titania nanoligands. With decreasing titania domain size, <10 nm, acidic activity increases and redox activity decreases due to their inverse electronic requirements. This is the first systematic study to demonstrate the ability of oxide nanoligands to tune the electronic structure and reactivity of surface metal oxide catalytic active sites.

1. Introduction

The potential impact of nanotechnology has generated renewed interest in nanoscale catalytic materials in recent years.[1−3] Early systematic studies with supported metal catalysts clearly demonstrated that nanosized metallic catalytic active sites can influence the catalytic performance of some structure-sensitive catalytic reactions.[4] For structure-sensitive reactions, the specific reactivity with decreasing domain size in the 1−10 nm range of the catalytic active sites can either increase (e.g., oxidation of H_2 to H_2O in excess H_2 over Pt catalysts) or decrease (e.g., synthesis of NH_3 from N_2 and H_2 over Fe catalysts). For structure-insensitive reactions, however, the specific catalytic activity is independent of the domain size of the metallic catalytic active site (e.g., hydrogenation of cyclohexene over Pt). These reactivity trends have been shown to be dependent on the nature of the interactions of the reactant molecules with the specific surface metal atom arrangements of the catalytic active sites.[4,5] For metal oxide catalytic materials, such a systematic examination and fundamental understanding of the influence of the domain size upon catalytic performance has yet to be established. The surface structure sensitivity of several specific catalytic reactions over metal oxide surfaces, however, is well documented in the literature.[4,6−10] This suggests that the domain size of metal oxide catalysts should also affect the reactivity of structure sensitive reactions. Such a fundamental framework for nanosized metal oxide catalysts is necessary for guiding the design of potentially novel and improved metal oxide catalytic active sites.

The objective of this report is to systematically examine and establish the reactivity trends, as well as their origins for *nanoscale* metal oxide catalytic active site domains for redox and acidic reactions. The metal oxide materials chosen for this investigation consist of well-defined, model-supported metal oxide catalysts. Supported metal oxide catalysts are composed of an amorphous two-dimensional surface metal oxide overlayer on an oxide substrate[11−13] and are extensively employed in the environmental, energy, and petrochemical industries.[14−16] For supported metal oxide catalytic materials involved in redox

---

[†] Department of Chemical Engineering, Lehigh University.
[‡] Department of Chemical and Biomolecular Engineering, Rice University.
[§] Departments of Materials Science and Engineering, Lehigh University.
[‖] Department of Chemistry, Rice University.

(1) Fernandez-Garcia, M.; Martinez-Arias, A.; Hanson, J. C.; Rodriguez, J. A. *Chem. Rev.* **2004**, *104*, 4063.
(2) Ogenko, V. M. *Adsorp. Sci. Technol.* **1996**, *14*, 295.
(3) Abbet, S.; Heiz, U. *Encycl. Nanosci. Nanotechnol.* **2004**, *6*, 161.
(4) Boudart, M., Djega-Mariadassou, G.; *Kinetics of Heterogeneous Catalytic Reactions*; Princeton University Press: Lawrenceville, 1984.
(5) Thomas, J. M., Thomas, W. J.; *Principles and Practice of Heterogeneous Catalysis*; VCH: Weinheim1997. Somorjai, G. A. *Introduction to Surface Chemistry and Catalysis*; Wiley: New York, 1994.
(6) Badlani, M.; Wachs, I. E. *Catal. Lett.* **2001**, *75*, 137.
(7) Tatibouet, J. M. *Appl. Catal. A: Gen.* **1997**, *148*, 213.
(8) Khodakov, A.; Olthof, B.; Bell, A. T.; Iglesia, E. *J. Catal.* **1999**, *181*, 205.
(9) Macht, J.; Baertsch, C. D.; May-Lozano, M.; Soled, S. L.; Wong, Y.; Iglesia, E. *J. Catal.* **2004**, *227*, 479.
(10) Farneth, W. E.; Ohuchi, F.; Staley, R. H.; Chowdhry, U.; Sleight, A. W. *J. Phys. Chem.* **1985**, *89*, 2493.
(11) Weckhuysen, B. M.; Wachs, I. E. *Handbook Surf. Interfaces Mater.* **2001**, *1*, 613.
(12) Wachs, I. E. *Catal. Today* **1996**, *27*, 437.
(13) Wachs, I. E. *Catalysis (Specialist Periodical Reports)* **1997**, *13*, 37.
(14) Thomas, C. T. *Catalytic Processes and Proven Catalysts*; Academic Press: New York, 1970.
(15) Weissermel, K.; Arpe, H.-J. *Industrial Organic Chemistry*; Verlag Chemie: Weinheim, 1978.

10.1021/ja711456c CCC: $40.75

reactions, the most significant parameter affecting the specific reactivity of the catalytic active site is the specific oxide support ligand (e.g., Al_2O_3, TiO_2, ZrO_2, etc.). The turnover frequency (TOF), defined as the number of molecules converted per catalytic active site per second, can vary by as much as $\sim 10^3$ for such catalytic systems when the specific oxide support ligand is varied.[13,17] Consequently, the influence of oxide nanoligand substrates upon the specific reactivity of redox and acidic catalytic active sites of supported metal oxide catalysts is the focus of this communication.

2. Experimental Section

2.1. Catalyst Synthesis. 2.1.1. Preparation of TiO_x/SiO_2 Catalysts. The silica support material, amorphous SiO_2 (Cabot, Cab-O-Sil fumed silica EH-5, S.A. $\approx$ 332 m^2/g), was employed and found to be more easily handled by an initial water pretreatment and calcination at 773 K for 4 h without changing the material properties. The TiO_2/SiO_2 supported oxide catalysts were prepared by the incipient-wetness impregnation of isopropanol solutions of titanium isopropoxide ($Ti(O{-}Pr^i)_4$, Alfa Aesar, 99.999%). The silica support was initially dried for 2 h at 393 K to remove the physisorbed water prior to catalyst preparation inside a glovebox (Vacuum Atmospheres, Omni-Laboratory VAC 101965) under a continuously flowing N_2 (Airgas, Ultra High Purity) environment. After impregnation at room temperature, the samples were kept inside the glovebox to dry overnight under flowing N_2. The calcination of the TiO_2/SiO_2 samples entailed ramping at 1 K/min to 393 K in flowing N_2 for 2 h, and then subsequently followed by another 1 K/min ramp under flowing air (Airgas, Zero grade) to 773 K for 4 h. A two-step preparation procedure was employed to prepare samples with loading higher than 8 wt % TiO_2. The second impregnation followed the same procedure described above using 8% TiO_2/SiO_2 as the starting material to prepare 10%, 12%, and 15% TiO_2/SiO_2 catalysts. Multiple impregnation steps were used to prepare samples with loadings higher than 15% TiO_2.

2.1.2. Preparation of $WO_x/TiO_2/SiO_2$ Catalysts. Highly dispersed (5 wt %) supported tungsten oxide catalysts were prepared by the incipient-wetness impregnation of aqueous solutions of ammonium metatungstate, $(NH_4)_{10}W_{12}O_{41} \cdot 5H_2O$ (Pfaltz and Bauer, 99.5% purity) on the various TiO_2/SiO_2 materials. The samples were dried overnight under ambient conditions and were subsequently dried in flowing air (Airgas, Zero grade) at 393 K for 1 h and calcined in flowing air (Airgas, Zero grade) at 723 K for 4 h.

2.1.3. Preparation of $VO_x/TiO_2/SiO_2$ Catalysts. Highly dispersed (5 wt %) supported vanadium oxide catalysts were prepared by the incipient-wetness impregnation of isopropanol solutions of vanadium triisopropoxide ($VO[CHO(CH_3)_2]_3$, Alfa Aesar, 97%) onto the various TiO_2/SiO_2 catalysts. The preparation was performed inside a glovebox with continuously flowing N_2 (Airgas, Ultra High Purity), and the TiO_2/SiO_2 support materials were initially dried at 393 K to remove the physisorbed water before impregnation. After impregnation at room temperature, the samples were kept inside the glovebox under flowing N_2 overnight. The calcination of the $VO_x/TiO_2/SiO_2$ samples entailed ramping at 1 K/min to 393 K in flowing N_2 for 2 h, and then subsequently followed by another 1 K/min ramp under flowing air (Airgas, Zero grade) to 773 K for 4 h.

2.2. Catalyst Characterization. 2.2.1. In Situ Raman Spectroscopy. Raman spectroscopy was used to obtain the molecular structures of the supported TiO_2/SiO_2, $VO_x/TiO_2/SiO_2$, and $WO_x/TiO_2/SiO_2$ catalysts with a visible (532 nm) laser excitation on a single stage Horiba−Jobin Yvon Laboratory Ram-HR Raman spectrometer equipped with a confocal microscope (Olympus BX-30) and a notch filter (Kaiser Super Notch). The visible excitation was generated by Nd:YAG doubled diode pumped laser (Coherent Compass 315M-150; output power of 150 mW with sample power 10 mW) with the scattered photons directed into a single monochromator and focused onto a UV-sensitive liquid-N_2 cooled CCD detector (Horiba-Jobin Yvon CCD-3000V) having a spectral resolution of ~ 2 cm^{-1} for the given parameters. The Raman spectrometer was also equipped with an environmentally controlled high-temperature environmental cell (Linkam, TS1500) that examined the catalyst samples in loose powder form ($\sim$5−10 mg) and also allowed for control of both the temperature and gaseous composition. In situ Raman spectra were collected for the supported tungsten oxide catalysts after dehydration at 723 K for 1 h in flowing 10% O_2/He (Airgas, certified, 9.735% O_2/He, ultrahigh purity and hydrocarbon-free, 30 mL/min) to desorb the adsorbed moisture and the spectra of the dehydrated samples were collected after cooling the catalysts back to 393 K in the flowing 10% O_2/He gas to ensure that the catalyst surface was void of moisture. The spectral acquisition time employed was 20 scans of 20 s/scan for a total of $\sim$7 min/spectrum. System alignment was verified daily using a silica reference standard provided by Horiba−Jobin Yvon.

2.2.2. In Situ CH_3OH Infrared (IR) Spectroscopy. In situ Fourier transform mid-infrared diffuse reflectance spectroscopy of chemisorbed methanol (CH_3OH-FTIR DRS) on supported TiO_2/SiO_2, $VO_x/TiO_2/SiO_2$, and $WO_x/TiO_2/SiO_2$ catalysts was performed by a purged single-beam Bio-Rad/Digilab Excalibur FTS4000 spectrometer equipped with KBr beamsplitter and DTGS detector. Undiluted powder samples were loaded into a Harrick Scientific cell (HVC-DRP3) with KBr windows and N_2-purged Praying Mantis chamber (DRP-XXX). An auxiliary thermocouple was installed just below the powder surface to measure catalyst temperature. Prior to each sample analysis, the diffuse reflectance accessories were adjusted with an alignment jig to provide >40% diffuse reflectance and specular reflectance less than 10% of the diffuse reflectance value at 2500 cm^{-1} compared to open beam path transmittance.

The sample procedure was developed from refs 18 and 19 and references within. Powders were heated to 673 K (15 K/min) for 30 min, oxidized in 100 mL/min dry air for 30 min to 673 K, cooled to 423 K in air to minimize thermal reduction[20] (although oxidation states were not experimentally verified), and cooled to 383 K under vacuum. After collecting a baseline spectrum of the pretreated virgin sample at 383 K in vacuum for the Kubelka−Munk reference, each sample was exposed to gas-phase methanol taken from the headspace of room-temperature liquid methanol under vacuum. After reaching surface saturation, the in situ cell was subsequently evacuated to remove weakly bound methoxy species. Next, infrared spectra were collected ever 5 min at a resolution of 2 cm^{-1} using 100 signal-averaged scans in the range 400−4000 cm^{-1} until no further spectral changes were observed. Only the final spectra, ratioed to their respective backgrounds, are included in the present report.

The Kubelka−Munk function[21] for infinitely thick samples was used to convert reflectance spectra into equivalent absorption spectra. For each respective catalyst sample, its virgin surface at 383 K after dehydration and oxidation but prior to methanol exposure was used as the reference spectrum.

2.2.3. In Situ UV−Vis Diffuse Reflectance Spectroscopy (DRS). The electronic structures of the TiO_x/SiO_2, catalysts were obtained with a Varian Cary 5E UV−vis spectrophotometer employing the integration sphere diffuse reflectance attachment (Harrick Praying Mantis Attachment, DRA-2). The finely ground

---

(16) Farrauto, R. J.; Bartholomew, C. H. Fundamentals of Industrial Catalytic Processes; Chapman and Hall: London, 1997.

(17) Wachs, I. E. *Catal. Today* **2005**, *100*, 79.

(18) Boreskov, G. K.; Muzykantov, V. S. *Ann. N.Y. Acad. Sci.* **1973**, *213*, 137.

(19) Davydov, A. A. *Molecular Spectroscopy of Oxide Catalyst Surfaces*; Wiley: Chichester, 2003.

(20) Goulding, M. R.; Thomas, C. B.; Hurditch, R. J. *Solid State Commun.* **1983**, *46*, 451.

(21) Kubelka, P.; Munk, F. *Z. Tech. Phys.* **1931**, *12*, 593.

powder catalyst samples (∼20 mg) were loaded into an in situ cell (Harrick, HVC-DR2) and measured in the 200−2200 nm region with a magnesium oxide reflectance standard used as the baseline. The UV−vis spectra of the supported catalysts were obtained after the samples were treated at 673 K for 1 h in flowing 10% O_2/He (Airgas, certified, 9.735% O_2/He, ultrahigh purity and hydrocarbon-free, 30 mL/min) to desorb the adsorbed moisture. Below 300 nm, the absorbance signal was unacceptably noisy and a filter (Varian, 1.5ABS) was employed to minimize the background noise. UV−vis DRS studies of the supported $MO_x/TiO_2/SiO_2$ catalysts were not successful in the present work, since absorption from the TiO_2 support exhibits strong absorption in the UV−vis region where VO_x and WO_x absorption occurs.

The UV−vis spectra were processed with Microsoft Excel software, consisting of the calculation of the Kubelka−Munk function, $F(R_\infty)$ which was extracted from the UV−vis DRS absorbance. The edge energy (E_g) for allowed transitions was determined by finding the intercept of the straight line in the low-energy rise of a plot of $[F(R_\infty)h\nu]^{1/n}$, where $n = 0.5$ for the direct allowed transition versus $h\nu$, where $h\nu$ is the incident photon energy.[21−23]

2.2.4. High Resolution-Transmission Electron Microscopy (HR-TEM). Samples for HR-TEM examination were prepared by dispersing the catalyst powder in high-purity ethanol, then allowing a drop of the suspension to evaporate on a lacy carbon film supported by a 300 mesh copper TEM grid. HR-TEM images of the ambient samples were obtained using a JEOL 2200FS transmission electron microscope, having an accelerating voltage of 200 kV, a point-to-point resolution of 0.19 nm, and an information limit of 0.11 nm. Fourier transform (FT) analyses of lattices fringe periodicities and interplanar angles were carried out using digital micrograph. Chemical analysis and EDS mapping were obtained using a VG 603 DSTEM.

2.3. Reactivity Studies. 2.3.1. Methanol-Temperature Programmed Surface Reaction (TPSR) Spectroscopy. Methanol-TPSR spectroscopy was performed on an AMI-200 temperature programmed system (Altamira Instruments) linked by a capillary tube to an online quadruple mass spectrometer (Dycor DyMaxion DME200MS, Ametek Process Instruments). Typically, ∼100 mg of catalyst was loaded in a U-type quartz tube and initially pretreated in flowing air at 723 K (Airgas, Ultra Zero grade Air, 30 mL/min) for 40 min to remove any possible adsorbed organic impurities and to dehydrate the sample. To ensure that the surface MO_x species remained in a fully oxidized state, the pretreated samples were initially cooled to 383 K, where the gas stream was switched to helium (Airgas, Ultra High Purity, 30 mL/min) to flush out any residual gas-phase O_2. The sample was further cooled to 373 K and held for 30 min to remove any physically adsorbed O_2 and background gases. At 373 K, methanol adsorption was performed by flowing 2000 ppm CH_3OH/He (Airgas, 30 mL/min) for 30 min, and then the system was purged with flowing helium (Airgas, Ultra High Purity, 30 mL/min) for another 30 min to remove any residual physically adsorbed methanol. Afterward, the sample was heated at a constant heating rate (10 K/min) to 773 K in flowing helium (Airgas, Ultra High Purity, 30 mL/min). The gases exiting from the quartz tube reactor were analyzed with the online mass spectrometer as a function of catalyst temperature. The following *m/e* ratios were employed for the identification of the various desoprtion gases: CH_3OH, *m/e* = 31; H_2CO, *m/e* = 30; CH_3OCH_3, *m/e* = 45 and 15(DME); CO, *m/e* = 28; CO_2, *m/e* = 44; H_2O, *m/e* = 18; H_3COOCH, *m/e* = 60(MF); and $(CH_3O)_2CH_2$, *m/e* = 75(DMM). For those desorbing molecules that gave rise to several fragments in the mass spectrometer, additional *m/e* values were also collected to further confirm their identity. The surface kinetic parameters (E_{act}, and k_{rds}) for the surface methoxy reactions to HCHO and CH_3OCH_3 are directly obtained from the CH_3OH-TPSR spectra. The rate-determining step (rds) for the unimolecular surface CH_3O^* dehydrogenation to HCHO involves breaking the surface methoxy C−H bond.[24] The rds for CH_3OCH_3 formation involves the unimolecular surface methoxy C−O bond scission.[25] The unimolecular aspect of the rds for the different reaction pathways allows application of the first-order Redhead equation to determine the E_{act} for the surface reactions:

$$\frac{E_{act}}{RT_p^{\,2}} = \left(\frac{\upsilon}{\beta}\right)\exp\left(\frac{-E_{act}}{RT_p}\right) \tag{1}$$

in which T_p is the CH_3OH-TPSR peak temperature of the reaction product, R is the gas constant (1.987 cal/mol·K), $\upsilon = 10^{13}$ s^{-1} for first-order kinetics,[24] and β is the heating rate (10 K/min). The rate determining steps, k_{rds} (DME) and k_{rds} (HCHO), of the surface methoxy intermediate conversion to DME and HCHO, respectively, are a function of E_{act} (and hence T_p) and determined by

$$k_{rds} = \upsilon \exp\left(\frac{-E_{act}}{RT}\right) \tag{2}$$

in which T is a reference temperature used for the comparison of k_{rds} values, in this case the T is the temperature at which the steady state methanol dehydrogenation studies are conducted.

2.3.2. Steady-State Methanol Dehydrogenation to Formalhyde and Dimethyl Ether. Steady-state methanol dehydrogenation experiments were conducted in an ambient-pressure reactor consisting of a single-pass downflow fixed bed quartz reactor (0.16 in. ID) packed with finely ground catalyst powder and quartz endcaps. Catalyst loadings (5−30 mg) were chosen to maintain total methanol conversion under 10%, permitting the assumption of differential (i.e., gradientless) reactor conditions. To mimic thermal resistance and estimate catalyst bed temperature, a thermocouple mounted at the same elevation as the catalyst bed was installed inside an identical quartz tube that was fixed to the reactor tube. Both tubes were mounted side-by-side snugly within a 0.5 in. ID metal tube wrapped in heat tape and insulation. Pretreatment consisted of calcining each catalyst at 623 K for 30 min in a 93 mL/min dry flowing gas mixture of Oxygen (Ultra High Purity, Airgas) and Helium (Ultra High Purity, Airgas) controlled at a molar O_2/He ratio of 14:79 by two independent Coriolis mass flow controllers. The reactor was then cooled to the desired reaction temperature (503 K for $VO_x/TiO_2/SiO_2$ catalysts and 573 K for $WO_x/TiO_2/SiO_2$ catalysts), and the feed gases were bubbled through a liquid methanol saturator (Alfa Aesar, ACS grade). The gas-phase methanol concentration was controlled by the temperature of an overhead condenser, operated at 281 K for these experiments. The final composition of the reactor feed stream was 7%:14%:79% CH_3OH/O_2/He at 100 mL/min total flow (ST = 273.15 K, 1 atm). Steady-state performance was determined by averaging 3−4 gas chromatograph (GC) cycles at the reaction temperature and comparing to initial 373 K temperature runs where each catalyst was consistently demonstrated inactive in converting methanol. Blank runs without the catalysts demonstrated negligible methanol conversion in the reactor system. The 0.25 in. OD stainless steel tubing from the reactor outlet to the GC was maintained between 393 and 423 K by heat tape and insulation to minimize condensation of the reactor effluents. The reactor effluent gases were analyzed by an HP5890 Series II online GC (Hewlett-Packard), operated in split mode (308 K for 6 min, ramp 20 K/min to 498 K hold for 5 min), with a 10-port Valco valve diverting two samples in parallel through a CP-sil 5CB capillary column (30 m × 0.32 mm × 5.0 μm, J & W Scientific) to the FID and a 40/60 Carboxene-1000 packed

---

(22) Gao, X.; Wachs, I. E. *J. Phys. Chem. B* **2000**, *104*, 1261.

(23) Delgass, W. N., Haller, G. L., Kellerman, R., Lunsford, J. H. *Spectroscopy in Heterogeneous Catalysis*; Academic Press: New York, 1979; p 86.

(24) Briand, L. E.; Farneth, W. F.; Wachs, I. E. *J. Catal.* **2002**, *208*, 301.

(25) Kim, T.; Burrows, A.; Kiely, C. J.; Wachs, I. E. *J. Catal.* **2007**, *246*, 370.

(26) Weber, R. S. *J. Catal.* **1995**, *151*, 470.

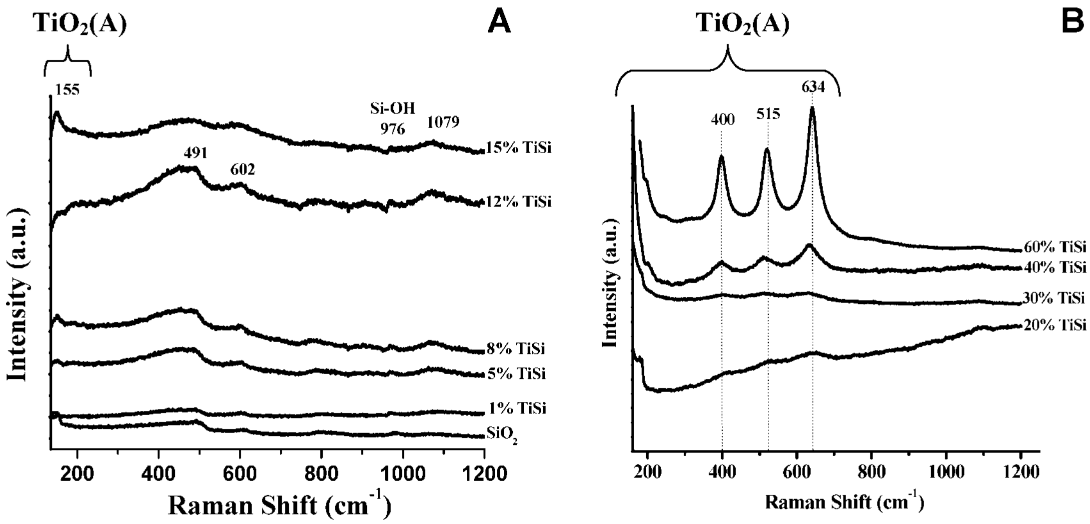

Figure 1. Raman spectra (532 nm) under dehydrated conditions as a function of TiO_2 loading of supported TiO_2/SiO_2 catalysts.

column (5 ft × 1/8 in., Supelco) and to the TCD for determination of the methanol conversion, selectivity, and activity. The steady-state methanol dehydrogenation catalytic data are expressed in terms of TOF, which represents the number of methoxy molecules converted per metal atom per unit time, as illustrated below

$$\mathrm{TOF} = \frac{R_{\mathrm{CH_3OH}}}{N_s S_{\mathrm{BET}}} \tag{3}$$

where the activity of each catalyst is expressed as the rate of methanol conversion, $R_{\mathrm{CH_3OH}}$, N_s represents the surface active site density, and the overall catalyst BET surface area is expressed as S_{BET}. Here N_s is equivalent to the metal oxide surface density assuming 100% exposure of all metal atoms, where surface density is expressed by the following

$$\rho_{\mathrm{surf}} = \frac{\left(\frac{\mathrm{wt\ \%\ MO}_x}{100}\right)\left(\frac{1}{M_{\mathrm{w}}\ \mathrm{MO}_x}\right)\upsilon_{\mathrm{stoich}}}{S_{\mathrm{BET}}} \tag{4}$$

3. Results and Discussion

3.1. Structural Characteristics of Supported $MO_x/TiO_2/SiO_2$ Catalysts. 3.1.1. Supported TiO_2/SiO_2 Catalysts. The Raman spectra of supported TiO_2/SiO_2 are presented in Figure 1. The XRD amorphous SiO_2 nanoparticles (NPs) possess weak Raman bands at ~400, ~490, ~602, and ~802 cm^{-1} originating from vibrations of 2,3,4-membered silica rings, and the band at ~975 cm^{-1} is associated with the Si−OH vibration, which decreases slightly with increasing TiO_2 content.[27] Raman bands associated with crystalline TiO_2(rutile) (142, 445, and 610 cm^{-1}), as well as crystalline TiO_2(brookite) (242, 320, 363, and 407 cm^{-1}) are not observed when TiO_2 is supported on the SiO_2 matrix.[27b] However, crystalline bulk TiO_2(anatase) which gives rise to strong Raman bands at 144, 400, 520, and 643 cm^{-1} are observed for samples containing high TiO_2 content (Figure 1). For samples with 12% TiO_2/SiO_2 or less, crystalline TiO_2(anatase) NPs are not present since their presence would give rise to strong Raman signals. Instead, the Raman spectrum of the 12% TiO_2/SiO_2 sample exhibits weak new Raman bands at ~920 and 1080 cm^{-1} characteristic of bridging Si−O···Ti bonds.[27] The silica surface Si−OH vibration at ~975 cm^{-1} is also slightly diminished by anchoring of titania on the SiO_2 substrate.[27] The reaction of titania with the silica surface hydroxyls, formation of the Si−O···Ti bonds and the absence

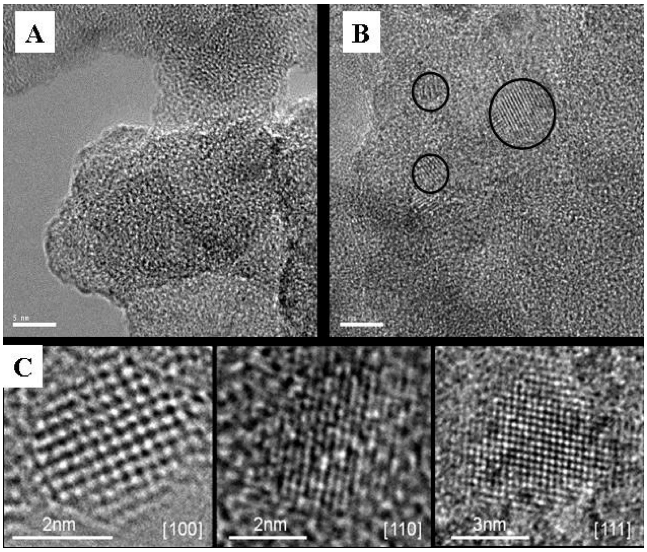

Figure 2. Representative HR-TEM images of TiO_2/SiO_2 containing (A) 12 wt % TiO_2 and (B) 30 wt % TiO_2 with red circles highlighting the crystalline TiO_2(anatase) NPs, along with (C) a selection HR-TEM images of nanoscale raftlike TiO_2 domains on the SiO_2 support, exhibiting fringe structures that are consistent with [100], [110], and [111] projections of the anatase phase.

Table 1. TiO_2 Domain Size for Supported TiO_2/SiO_2 Catalysts as Determined by HR-TEM

catalyst	structure	domain size (nm)
1% TiO_2/SiO_2	isolated surface TiO_4 species	~0.4[a]
5% TiO_2/SiO_2	isolated surface TiO_4 and polymeric surface TiO_5 species	−
12% TiO_2/SiO_2	polymeric surface TiO_5 species	~1[b]
20% TiO_2/SiO_2	polymeric surface TiO_5 species and TiO_2(A)	2−4
30% TiO_2/SiO_2	TiO_2(A)	3−5
40% TiO_2/SiO_2	TiO_2(A)	5−9

[a] Estimated for isolated TiO_4 unit. [b] Estimated for a chain of three surface TiO_5 units.

---

(27) Gao, X.; Bare, S. R.; Fierro, J. L.; Banaras, M. A.; Wachs, I. E. *J. Phys. Chem. B* **1998**, *102*, 5653. (b) Deo, G.; Turek, A. M.; Wachs, I. E. *Appl. Catal. A: Gen.* **1992**, *91*, 27.

Scheme 1. Molecular Structures of Different TiO_2 Domains (A) Isolated Surface TiO_4, (B) Polymeric Surface TiO_5, and (C) Crystalline TiO_2(anatase) Having TiO_6 Octahedral Units

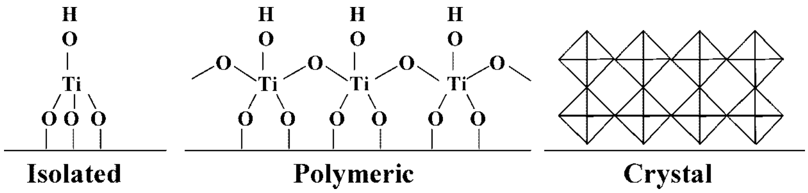

of TiO_2 (anatase) crystallites reflect the presence of a two-dimensional surface TiO_x layer on the SiO_2 support below 12% TiO_2/SiO_2. Thus, the SiO_2-supported TiO_2/SiO_2 materials only contain surface TiO_x species for 12% TiO_2/SiO_2 and lower loading and TiO_2(anatase) NPs of varying dimension above 12% TiO_2/SiO_2 loading. Complementary in situ XANES revealed that the dehydrated 1% TiO_2/SiO_2 sample consists of isolated surface TiO_4 species on the silica support and that the dehydrated 12% TiO_2/SiO_2 sample contains polymeric surface TiO_5 species on the silica substrate.[27]

Additional structural information about the SiO_2-supported titania phase was provided by HR-TEM studies and representative images for the 12% TiO_2/SiO_2 sample, possessing the polymeric surface titania layer, and the 30% TiO_2/SiO_2 sample, containing the crystalline titania particles are shown in panels A and B of Figure 2, respectively. The support material primarily consists of ~15 nm amorphous, roughly spherical SiO_2 nanoparticles (NPs) with some minor fraction of the particles being as large as 30 nm. For the 12% TiO_2/SiO_2 sample (Figure 2A), crystalline TiO_2 particles are not observed, which is consistent with the Raman findings above. Bright field diffraction contrast imaging and selected area electron diffraction patterns also showed no discernible signs of crystalline TiO_2. However, energy dispersive X-ray spectroscopy (XEDS) on the 12% TiO_2/SiO_2 sample did confirm the presence of titanium atoms on the support. Crystalline TiO_2 NPs, about 3−5 nm in size, are observable by their characteristic fringe patterns in the 30% TiO_2/SiO_2 sample (Figure 2B). Interestingly, the TiO_2 NPs form with a raftlike morphology on the silica support, as evidenced by the fact they were never seen in profile. FT analysis of those patches that exhibited crossed lattice fringes was carried out in order to measure the lattice spacing and interplanar angles of these crystalline domains. In the majority of cases, the fringe patterns could be matched to the anatase phase of TiO_2. A few typical examples of such patches, consistent with the [100], [110], and [111] projections of anatase are shown in Figure 2C. The formation of the TiO_2 (anatase) NPs in the 30% TiO_2/SiO_2 sample was found to consume the surface TiO_x species since no discernible titanium signal could be detected by XEDS from the SiO_2 support regions between the TiO_2 NPs. The transformation occurs because of the greater affinity of the surface TiO_x species for the TiO_2 (anatase) NPs over the relatively inert SiO_2 surface. The titania domain size of the different supported TiO_2/SiO_2 samples is listed in Table 1, and the molecular structures are shown illustratively in Scheme 1. Such novel raft structures possess properties unlike the typical 3D TiO_2 (anatase) NPs (see below).

The corresponding electronic structures of the series of supported TiO_2/SiO_2 samples possessing variable titania nanodomain size were examined with in situ UV−vis spectroscopy. UV−vis DRS exclusively provides information about the local electron density of the supported titania phase because of the weak absorbance by the SiO_2 support.[28] The electron density of nanostructured metal oxide clusters is known to be dependent on the metal oxide domain size, with the local electron density increasing for smaller dimensions and the electrons becoming more delocalized for larger dimensions.[26] The edge energy, E_g (eV), values for the different supported titania materials increase continuously as the TiO_x domain size decreases as shown in Figure 3. Larger edge energy values correspond to higher local electron density and less electron delocalization, which also generally corresponds to a less reducible metal oxide. This trend reflects the well-known quantum confinement effect for small dimensions.[29]

In summary, the chosen synthesis method successfully varied the SiO_2-supported titania domain size over a wide range, in the critical sub-10 nm domain size, that would allow for examination of the oxide nanoligand substrate domain size upon the structure and reactivity of different types of supported catalytic active sites. It is, thus, anticipated that redox reactions that require electrons should be favored by large domain size and acidic reactions that do not require electrons should be favored by small domain size.[4,30,31]

3.1.2. Supported $WO_x/TiO_2/SiO_2$ Catalysts. The molecular nature of the deposited tungsten oxide phase on the TiO_2/SiO_2 support was determined with in situ Raman spectroscopy, and the spectra are presented in Figure 4. The Raman spectra reveal that crystalline WO_3 NPs are not present (absence of strong bands at 804, 710,and 270 cm^{-1}) and, consequently, that the active tungsten oxide is 100% dispersed as surface WO_x species on the TiO_2/SiO_2 support (Raman bands in the ~1000 cm^{-1} range).[12] The broad Raman band at ~1080 cm^{-1} is associated with the bridging Ti−O−Si vibration and is not related to the surface WO_x vibrations. For dehydrated WO_3/SiO_2, the primary Raman W=O vibration occurs at ~980 cm^{-1}, characteristic of dioxo (O=W=O) WO_4 species,[32] with a weaker vibration at ~1010 cm^{-1}, associated with monoxo (W=O) WO_5 species.[12,32−36] The Raman spectra for all of the dehydrated supported $WO_x/TiO_2/SiO_2$ catalysts, however, are dominated by the monoxo W=O vibration at ~1010 cm^{-1}. The constant vibration of the W=O bond with titania content indicates that the molecular structure of the surface WO_x species is the same for all supported TiO_2/SiO_2 catalysts. The position of this Raman band also reveals that the surface WO_x species preferentially coordinate to TiO_x sites rather than SiO_2 sites and the titania nanoligand

---

(28) Gao, X.; Wachs, I. E. *J. Phys. Chem. B* **2000**, *104*, 1261.
(29) Fernandez-Garcia, M. *Catal. Rev.* **2002**, *44*, 1.
(30) Liu, H.; Cheung, P.; Iglesia, E. *J. Catal.* **2003**, *217*, 222.
(31) Chen, M. S.; Goodman, D. W. *Science* **2004**, *306*, 252.
(32) Lee, E.; Wachs, I. E. *J. Phys. Chem. C.* **2007**, *111*, 14410–14425.
(33) Kim, D. S.; Ostromecki, M.; Wachs, I. E. *J. Mol. Catal. A Chem.* **1996**, *106*, 93.
(34) Vuurman, M. A.; Wachs, I. E. *J. Phys. Chem.* **1992**, *96*, 5008.
(35) Jarupatrakorn, J.; Coles, M. P.; Tilley, T. D. *Chem. Mater.* **2005**, *17*, 818.
(36) Nakamoto, K. *Infrared and Raman Spectra of Inorganic Coordination Compounds*, 5th ed.; Wiley and Sons: New York, 1997.

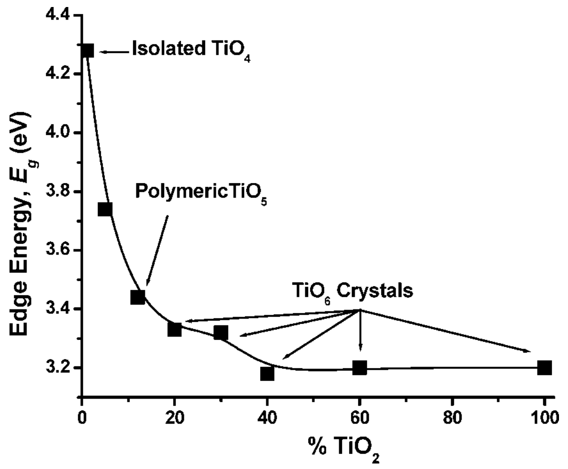

Figure 3. UV−vis edge energy, E_g (eV), as a function of % TiO_2 loading for supported TiO_2/SiO_2 catalysts.

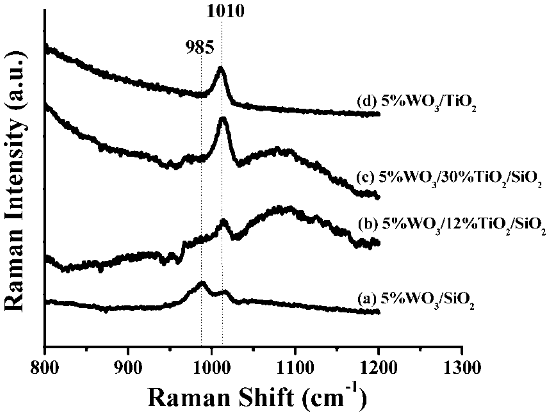

Figure 4. Raman Spectra (532 nm) under dehydrated conditions for (A) 5% WO_3/SiO_2, (B) 5% WO_3/12% TiO_2/SiO_2, (C) 5% WO_3/30% TiO_2/SiO_2, and (D) 5% WO_3/TiO_2.

alters the surface WO_x molecular structure. This preferential binding of surface WO_x to the TiO_x nanoligand over the SiO_2 support sites was further confirmed by methanol IR chemisorption studies that discriminated between surface Si−OCH_3, Ti−OCH_3, and W−OCH_3 vibrations and are presented in Figure 5. The CH_3OH-IR spectra demonstrate that the Ti−OCH_3 IR bands (2920 and 2822 cm^{-1}) are significantly diminished relative to the Si−OCH_3 IR bands in the presence of surface W-OCH_3 species because the surface WO_x sites are preferentially coordinated to the surface titania nanoligands. Note that the Ti-OCH_3 IR vibrations are almost absent for the 5% WO_3/x% TiO_2/SiO_2 catalysts and that ~5% WO_x covers ~5% TiO_2. The preferential anchoring of WO_x on TiO_x is related to the higher surface free energy of titania relative to silica, and the facile surface diffusion of surface WO_x at modest temperatures. The thermodynamic driving force is lowering of the system surface free energy (replacing higher free energy surface Ti−OH bonds with lower surface free energy terminal W=O bonds) and the kinetics are facilitated by surface diffusion of the metal oxides (related to the modest WO_3 Tammann temperature[35,37]). Thus, both location and structure of surface WO_x species are controlled by the titania nanoligands and the surface WO_x structure is independent of titania loading.

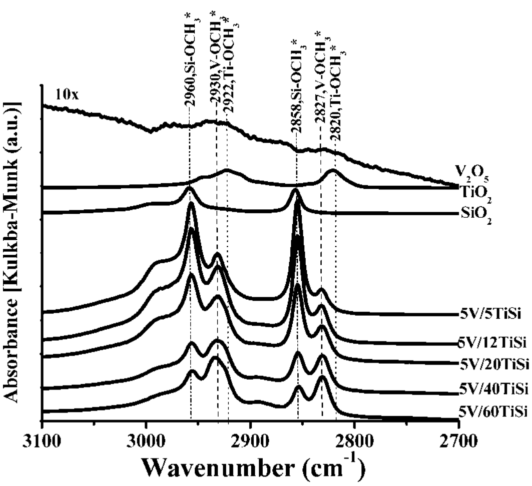

Figure 5. Infrared spectra of adsorbed methoxylated surface species in the C−H stretching region for 5%WO_x/x%TiO_2/SiO_2 catalysts.

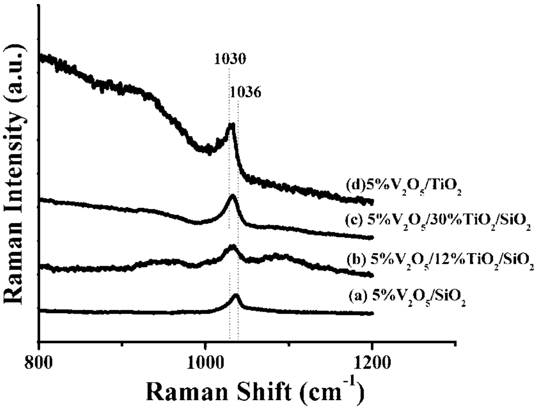

Figure 6. Raman spectra (532 nm) under dehydrated conditions for (A) 5% V_2O_5/SiO_2, (B) 5% V_2O_5/12% TiO_2/SiO_2, (C) 5% V_2O_5/30% TiO_2/SiO_2, and (D) 5% V_2O_5/TiO_2.

3.1.3. Supported $VO_x/TiO_2/SiO_2$ Catalysts. The nature of the dehydrated supported vanadia phase on the TiO_2/SiO_2 support was determined with in situ Raman spectroscopy and the spectra are shown in Figure 6. The Raman spectra reveal that crystalline V_2O_5 NPs are not present (absence of strong band at 994 cm^{-1}) and that the surface VO_x species is 100% dispersed on the TiO_2/SiO_2 support (Raman band ~1036 cm^{-1}).[39] Previous XANES and solid-state ^{51}V NMR characterization revealed that the dehydrated surface VO_x species always possessed VO_4 coordination.[39−42] For the dehydrated supported V_2O_5/SiO_2 catalyst, the Raman band of the monoxo surface VO_4 species vibrates at ~1036−1040 cm^{-1}.[39] For the dehydrated supported V_2O_5/TiO_2 catalyst, the monoxo surface VO_4 species band appears at ~1027−1031 cm^{-1}.[42] The surface VO_4 species, unlike the surface WO_x species, always possess the monoxo V=O structure and do not change coordination with different support ligands.[40,41] Nevertheless, there is a slight shift in the terminal V=O bond

---

(37) Knözinger, H.; Taglauer, E. Spreading and Wetting. In *Preparation of Solid Catalysts*; Ertl, G., Knözinger, H., Weitkamp, J., Eds.; Wiley-VCH: Weinheim, 1999.

(38) Knozinger, H.; Taugler, E. *Catalysis (Specialist Periodical Reports)* **1993**, *10*, 1.

(39) Gao, X.; Bare, S. R.; Weckhuysen, B. M.; Wachs, I. E. *J. Phys. Chem. B* **1998**, *102*, 10842.

(40) Eckert, H.; Wachs, I. E. *J. Phys. Chem.* **1989**, *93*, 6796.

(41) Das, N.; Eckert, H.; Hu, H.; Wachs, I. E.; Walzer, J. F.; Feher, F. *J. Phys. Chem.* **1993**, *97*, 8240.

(42) Gao, X.; Bare, S. R.; Wachs, I. E. *J. Phys. Chem. B* **1999**, *103*, 618.

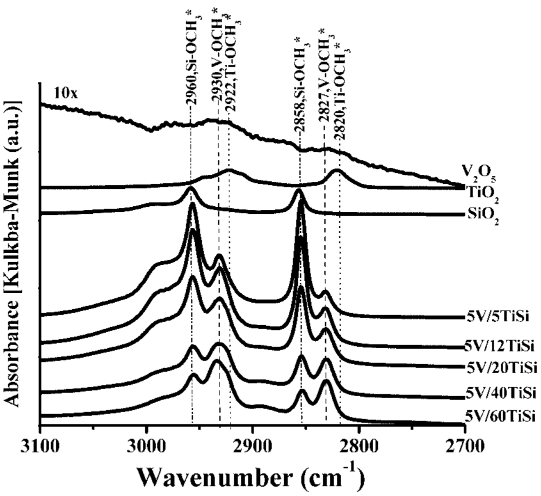

Figure 7. Infrared spectra of adsorbed methoxylated surface species in the C−H stretching region for 5%VO_x/*x*%TiO_2/SiO_2 catalysts.

when it is coordinated to different oxide support ligands.[43] The Raman band of the terminal V=O bond at ~1032 cm^{-1} reflects the preferential coordination of the surface VO_4 species to the supported titania phase over the silica support. This is further confirmed by CH_3OH-IR spectra that demonstrate the preferential anchoring of the surface VO_4 species on the titania sites (see Figure 7), since Ti−OCH_3 IR vibrations (2922 and 2820 cm^{-1}) are almost absent from the 5% V_2O_5/*x*% TiO_2/SiO_2 catalysts reflecting that the Ti sites are preferentially being covered by the surface VO_x species. In situ X-ray absorption near edge spectroscopy (XANES) results are also consistent with the preferential coordination of the surface VO_4 species to the titania nanoligands since the polymeric surface TiO_5 species increase their coordination to TiO_6 with anchoring of the surface vanadia.[42] Furthermore, the relatively constant Raman band at ~1032 cm^{-1} indicates that the same surface VO_x species are present for all the TiO_2/SiO_2 samples. Thus, similar to the supported WO_x/TiO_2/SiO_2 catalyst system, the catalytic active surface VO_4 species preferentially anchor or self-assemble at the surface titania sites.

3.2. Catalytic Properties of Supported MO_x/TiO_2/SiO_2 Catalysts. 3.2.1. Supported WO_x/TiO_2/SiO_2 Catalysts. The surface catalytic chemistry of the new monoxo surface WO_5 species bonded to the titania nanoligands catalysts was chemically probed with CH_3OH dehydration to CH_3OCH_3 and H_2O, which only takes place over surface acidic catalytic active sites.[6,7] Unlike the redox character of the dioxo surface WO_4 species on SiO_2 that yield H_2CO, the monoxo surface WO_5 species on TiO_2/SiO_2 behave as acidic sites since they exclusively yield DME as the reaction product. Methanol dehydration to dimethyl ether proceeds via the following elementary reaction steps:

$$CH_3OH + * + O* \leftrightarrow CH_3O* + HO* \qquad (1)$$

$$CH_3O* + * \rightarrow CH_3* + O* \qquad \text{(rds)} \qquad (2)$$

$$CH_3* + CH_3O* \rightarrow CH_3OCH_3 \qquad (3)$$

$$HO* + HO* \rightarrow H_2O + * + O* \qquad (4)$$

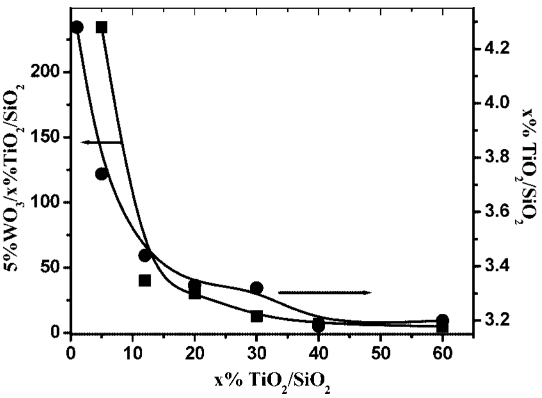

Figure 8. First-order rate constant for C−O bond breaking of the surface CH_3O* intermediate in formation of CH_3OCH_3 and titania nanoligand E_g as a function of titania loading for the supported 5% WO_3/*x*% TiO_2/SiO_2 catalyst system.

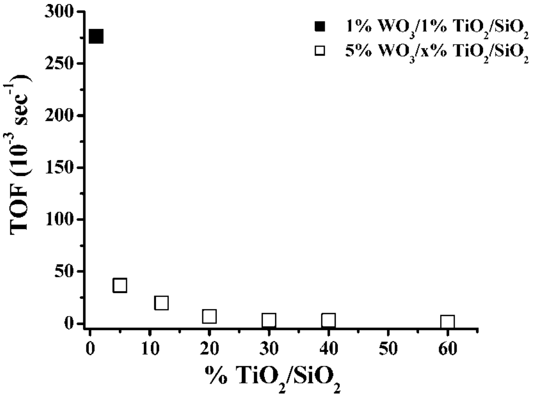

Figure 9. Catalytic acidity, TOF, for CH_3OH dehydration to DME over 5% WO_x/*x*% TiO_2/SiO_2 catalysts as a function of TiO_2 loading for a steady-state reaction temperature of 573 K.

with the breaking of the C−O bond representing the first-order rds. The asterisk represents an empty or uncoordinated W site, whereas X* represents an occupied surface W site (X = O*, HO*, CH_3*, or CH_3O*).[4] The overall reaction stoichiometry is given by

$$2CH_3OH \rightarrow CH_3OCH_3 + H_2O \qquad (5)$$

and shows that oxygen from the catalytic active surface WO_5 sites is not consumed in this surface acidic reaction. The CH_3OH dehydration reaction over the supported WO_3/TiO_2/SiO_2 catalysts was found to be 100% selective toward CH_3OCH_3 formation. This reflects the catalytic dominance of the acidic surface WO_x sites in these catalysts. The first-order reaction rate constants for scission of the C−O bond on the supported WO_3/TiO_2/SiO_2 catalysts were determined with CH_3OH-TPSR spectroscopy[44] and are compared with the corresponding titania E_g values as a function of the catalyst titania content in Figure 8. The monotonic increase in k_{rds} with decreasing domain size follows almost the exact same trend as the E_g values of the titania nanoligands as a function of titania domain size. Similar trends were also obtained for steady-state CH_3OH dehydration over the supported WO_3/TiO_2/SiO_2 catalysts as a function of the titania nanoligand domain size (Figure 9). These findings reveal that higher E_g values of the titania nanoligand, with less electron delocalization, correspond to enhanced acidic activity of the surface WO_5 catalytic active sites. Thus, small TiO_2 domains decrease the extent of electron delocalization and enhance the catalytic activity of nonreducible catalytic acid sites. *This is direct evidence for the influence of nanostructured oxide*

---

(43) Deo, G.; Wachs, I. E. *J. Catal.* **1994**, *146*, 335.

(44) Wang, X.; Wachs, I. E. *Catal. Today* **2004**, *96*, 211.

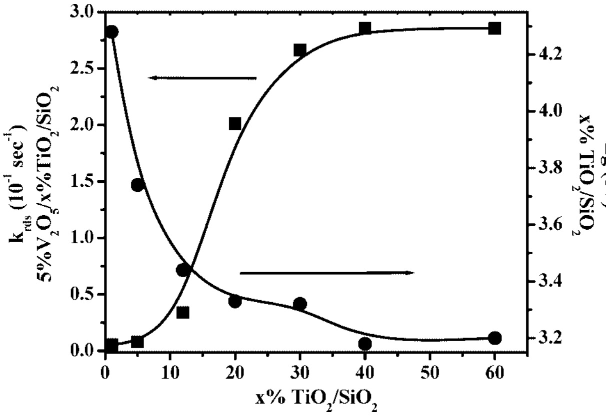

Figure 10. First-order rate constant for C−H bond breaking of the surface CH_3O^* intermediate in formation of HCHO and titania nanoligand E_g as a function of titania loading for the supported 5% V_2O_5/*x*% TiO_2/SiO_2 catalyst system.

support dimension and E_g *on catalytic activity of surface acidic sites.*[25]

3.2.2. Supported $VO_x/TiO_2/SiO_2$ Catalysts. The surface catalytic chemistry of the surface VO_4 species on the titania nanoligands was chemically probed with CH_3OH oxidation to HCHO and H_2O, which only takes place on surface redox catalytic active sites.[6,7,45] Formation of CH_3OCH_3 was not observed, which reflects the dominance of the redox nature of the surface VO_4 species. Methanol oxidation to formaldehyde proceeds via the following elementary reaction steps:

$$CH_3OH + O* + * \leftrightarrow CH_3O* + HO* \qquad (6)$$

$$CH_3O* \rightarrow HCHO + H* \qquad \text{(rds)} \qquad (7)$$

$$H* + HO* \leftrightarrow H_2O + 2* \qquad (8)$$

with the breaking of the C−H bond of the surface CH_3O^* intermediate representing the first-order rds. The overall reaction stoichiometry is given by eq 9, which shows that oxygen from the catalytic active surface VO_4 species is consumed in this surface redox reaction.

$$CH_3OH + {}^1\!/_2O_2 \rightarrow HCHO + H_2O \qquad (9)$$

The consumption of one oxygen atom is accompanied by the reduction of the surface vanadia species by two electrons:

$$V^{+5} + 2e^- \rightarrow V^{+3} \text{ or } 2V^{4+} \qquad (10)$$

The first-order reaction rate constants for breaking of the C−H bond of the surface CH_3O^* intermediates were determined with CH_3OH-TPSR [44,45] and are compared with the E_g values of the titania nanoligands as a function of the titania content in the catalysts, as shown in Figure 10. The monotonic decrease in k_{rds} with decreasing titania domain size varies inversely to the increasing E_g value of the titania nanoligands. Similar trends were also obtained for steady-state methanol oxidative dehydrogenation over the supported $VO_x/TiO_2/SiO_2$ catalysts as a function of the titania nanoligand domain size (Figure 11). These findings reveal that lower E_g values, with greater electron delocalization, correspond to enhanced redox activity of surface VO_4 catalytic active sites. Thus, large TiO_2 domains increase the extent of electron delocalization and enhance the catalytic activity of the reducible catalytic redox sites.

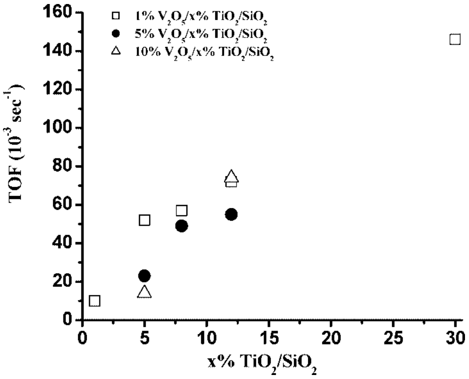

Figure 11. Catalytic activity, TOF, for CH_3OH oxidative dehydrogenation to HCHO over 5% VO_x/*x*% TiO_2/SiO_2 catalysts as a function of TiO_2 loading for a steady-state reaction temperature of 503 K.

4. Conclusions

Titania nanoligands, in the sub-10 nm range, with variable electronic structures were successfully synthesized on a relatively inert SiO_2 support. The catalytic active surface redox (VO_x) and acidic (WO_x) sites were found to preferentially self-assemble at the titania nanoligands in the mixed TiO_2/SiO_2 support materials. For surface redox sites, *increasing* the domain size of the titania nanoligands significantly *enhances* the specific catalytic activity by delocalization of the titania electrons. For the surface acidic sites, in contrast, *decreasing* the titania domain size significantly *enhances* the catalytic activity by localization of the titania electrons. The inverse responses of surface redox and surface acidic sites to the electron density of the titania nanoligands reflect the different reactivity requirements of surface redox and surface acidic metal oxide catalytic active sites. This is the first direct evidence for the influence of nanostructured oxide support dimension and optical E_g values on the catalytic activity of surface MO_x sites. In spite of the incomplete control of the TiO_2 domain size, which is intrinsic to the conventional catalyst impregnation route employed, these experimental findings clearly demonstrate that the catalytic active monoxo surface WO_5 and VO_4 species coordinate to the TiO_2 domains on SiO_2. Thus, varying the local electron density of oxide nanoligand supports allows for the tuning of the specific activity characteristics of surface metal oxide catalytic active sites as shown for the supported $VO_x/TiO_2/SiO_2$ and $WO_x/TiO_2/SiO_2$ catalyst systems.

Acknowledgment. The authors gratefully acknowledge the financial support by the NSF NIRT Grant No. 0609018. M.S.W. also acknowledges 3M (NFT Award) for financial support.

JA711456C

---

(45) Kim, T.; Wachs, I. E. *J. Catal.* **2008**, *255*, 197.